JOURNAL OF SOLID STATE CHEMISTRY **132,** 420–431 (1997)
ARTICLE NO. SC977484

A Bismuth Manganite with the "2212" Structure: $Bi_{2-x}Pb_xSr_{1.5}Ca_{1.5}Mn_2O_{9-\delta}$

M. Hervieu, C. Michel, D. Pelloquin, A. Maignan, and B. Raveau

Laboratoire de Cristallographie et Sciences des Matériaux, ISMRA-Université de Caen, Boulevard du maréchal Juin, 14050 Caen Cedex, France

Received January 9, 1997; in revised form May 16, 1997; accepted May 22, 1997

A manganite $Bi_{2-x}Pb_xSr_{1.5}Ca_{1.5}Mn_2O_{9-\delta}$, with the 2212 structure, has been synthesized for the first time. Its structural study by powder X-ray diffraction and by electron microscopy has been performed for two compositions, $x = 0.5$ and $x = 1$. The average structure consists of double perovskite layers (P) involving MnO_6 octahedra and MnO_5 pyramids intergrown with distorted triple rock salt layers (RS). The perovskite cages are mainly occupied by strontium so that these phases can be formulated $[Bi_{2-x}Pb_xCa_{1.33}Sr_{0.67}]_{RS}[Sr_{0.83}Ca_{0.17}]_PMn_2O_{9-\delta}$. The HREM investigation shows that the composition $x = 0.5$ exhibits an incommensurate modulated structure similar to that observed for the superconducting bismuth cuprate and for the iron-based 2212 compound. In contrast, the composition $x = 1$ does not exhibit any modulation. Although they are rare, some extended defects are observed especially for $BiPbSr_{1.5}Ca_{1.5}Mn_2O_{9-\delta}$. Both oxides are semiconductors. © 1997 Academic Press

INTRODUCTION

The exploration of transition metal oxides with a layered structure has become a very important topic since the discovery of superconductivity at high temperature in layered cuprates. The understanding of the relationships between magnetism and superconductivity in these materials requires the study of isotypic series, involving different transition elements, such as copper, iron, cobalt, and manganese. In this respect, the bismuth compounds are of high interest. Two series of magnetic oxides were indeed synthesized besides the superconductors $Bi_2Sr_2Ca_{m-1}Cu_mO_{2m+4+\delta}$. They correspond to the generic formulation $Bi_2(Sr, Ca)_{m+1}M_mO_{3m+3\pm\delta}$, with $m = 1, 2, 3$ for $M =$ Fe (1–3) and $m = 1, 2$ for $M =$ Co (3, 4). Despite their different formulations, all these oxides have closely related structures, so that they can be considered as practically isotypic. They can indeed be described as intergrowths of distorted triple rock salt layers with multiple perovskite layers. A major common structural point is that they all exhibit similar phenomena of incommensurate modulations (1–6). The main structural difference between the cuprates and the other compounds concerns the appearance of ordered oxygen vacancies in the perovskite layers, leading to a different oxygen content.

In contrast to iron and cobalt, only one manganese member belonging to the above series, $Bi_2Sr_2MnO_{6+\delta}$ (7), could be synthesized to date. The recent discovery of giant magnetoresistance (GMR) properties in manganese perovskites has renewed our interest for those compounds. The study of such materials is all the more attractive since the issue of the influence of the dimensionality of the structure upon the GMR properties is so far not understood. Clearly, such properties appear in a great number of $Ln_{1-x}A_xMnO_3$ perovskites (8–11), whereas only some layered manganites such as $Ln_{1+x}Sr_{2-x}Mn_2O_7$, $Ln =$ La, Pr, Nd (12), exhibit GMR properties. For these reasons, we have reinvestigated the system Bi–Pb–Sr–Ca–Mn–O, trying to synthesize the second member of the series $Bi_2(Sr, Ca)_{m+1}MnO_{3m+3+\delta}$. In the present paper, we report on the synthesis and on the complex crystal chemistry of the new phase $Bi_{2-x}Pb_xSr_{1.5}Ca_{1.5}Mn_2O_9$ that is obtained for $0.5 \leq x \leq 1$.

EXPERIMENTAL

Polycrystalline samples of 2212 manganese oxides were prepared according to the general compositions $Bi_{2-x}Pb_xSr_{2-y}Ca_{1+y}Mn_2O_{9-\delta}$, varying x and y from 0 to 1. Stoichiometric mixtures of Bi_2O_3, PbO, $SrCO_3$, CaO, and Mn_2O_3 were homogenized in an agate mortar, pressed in the form of bars, and heated under nitrogen flow, at 900°C, for 24 hr.

The powder X-ray diffraction (PXRD) patterns were registered by step scanning over an angular range of $10° \leq 2\theta \leq 80°$ with an increment of 0.02° (2θ), with a Philips diffractometer using Cu$K\alpha$ radiation. Parameter refinements were carried out using the Rietveld method (13) (program FULLPROF (14) Version 3.2).

The electron diffraction (ED) study was carried out with a Jeol 200CX electron microscope fitted with an eucentric goniometer ($\pm 60°$). The high-resolution electron microscopy (HREM) study was performed with a TOPCON 002B electron microscope, having a point resolution of

0022-4596/97 $25.00

1.8 Å. Both microscopes are equipped with Kevex analyzers for energy dispersive spectrometry (EDS). Samples selected for electron microscopy were obtained by crushing the material in alcohol and dispersing the flakes on a holey carbon copper or nickel grid. A major difficulty was the strong anisotropy of most of the samples; the overwhelming majority of the crystals were indeed oriented with the [001] axis parallel to the electron beam, as usually observed in bismuth cuprates.

The physical properties were studied by electrical resistivity measurements (four probe method) between 20 and 273 K.

RESULTS

Strategy of the Synthesis

The systematic investigation of the system Bi–Pb–Sr–Ca–Mn–O, first made with the nominal composition $Bi_{2-x}Pb_xSr_{2-y}Ca_{1+y}Mn_2O_{9-\delta}$, shows that, whatever $x > 0.1$, an optimum Sr/Ca ratio equal to 1 is required to avoid the formation of the very stable 2201 phase $Bi_{2-x}Pb_xSr_2MnO_{6+\delta}$ (15). Then, on this basis the best results are obtained, for the formulation $Bi_{2-x}Pb_xSr_{1.5}Ca_{1.5}Mn_2O_{9-\delta}$, with $0.50 \leq x \leq 1$. Nevertheless, even for those compositions, one always observes, besides the main 2212 phase, a secondary phase with the perovskite structure $Sr_{0.5}Ca_{0.5}MnO_{3-\delta}$, whose amount can be estimated at less than 10%.

The EDS analyses performed for numerous crystallites of the $x = 0.5$ and $x = 1$ samples show that the average actual compositions of the grains are close to the nominal ones, i.e., $Bi_{1.5}Pb_{0.5}Sr_{1.5}Ca_{1.5}Mn_2O_{9-\delta}$ and $BiPbSr_{1.5}Ca_{1.5}Mn_2O_{9-\delta}$, respectively. However, one sometimes observes either a small (Bi + Pb) deficiency, 0.1 maximum per cell, or local variations of the Bi/Pb ratio within one crystal core; this point will be further discussed.

Electron Diffraction

The electron diffraction investigation was performed on the two limits $x = 0.50$ and $x = 1$, showing that the first exhibits a modulated structure whereas the second is not modulated.

$Bi_{1.5}Pb_{0.5}Sr_{1.5}Ca_{1.5}Mn_2O_{9-\delta}$. The reconstruction of the reciprocal space shows that the orthorhombic basic cell parameters are $a \approx b \approx a_p\sqrt{2}$ and $c \approx 31$ Å. The conditions limiting the reflection are hkl, $k + l = 2n$ and $0kl$, k, and $l = 2n$, which are consistent with the space groups $Abm2$ and $Abmm$. The [001] and [010] ED patterns are given in Figs. 1a and 1b. The intense reflections are indexed in the A-type cell. The basis cell parameters were refined from the PXRD data to $a = 5.3594(1)$ Å, $b = 5.3443(1)$ Å, and $c = 30.976(4)$ Å (Table 1). Note that the c parameter is slightly larger than that of the cuprate $Bi_2Sr_2CaCu_2O_8$, despite the higher calcium content.

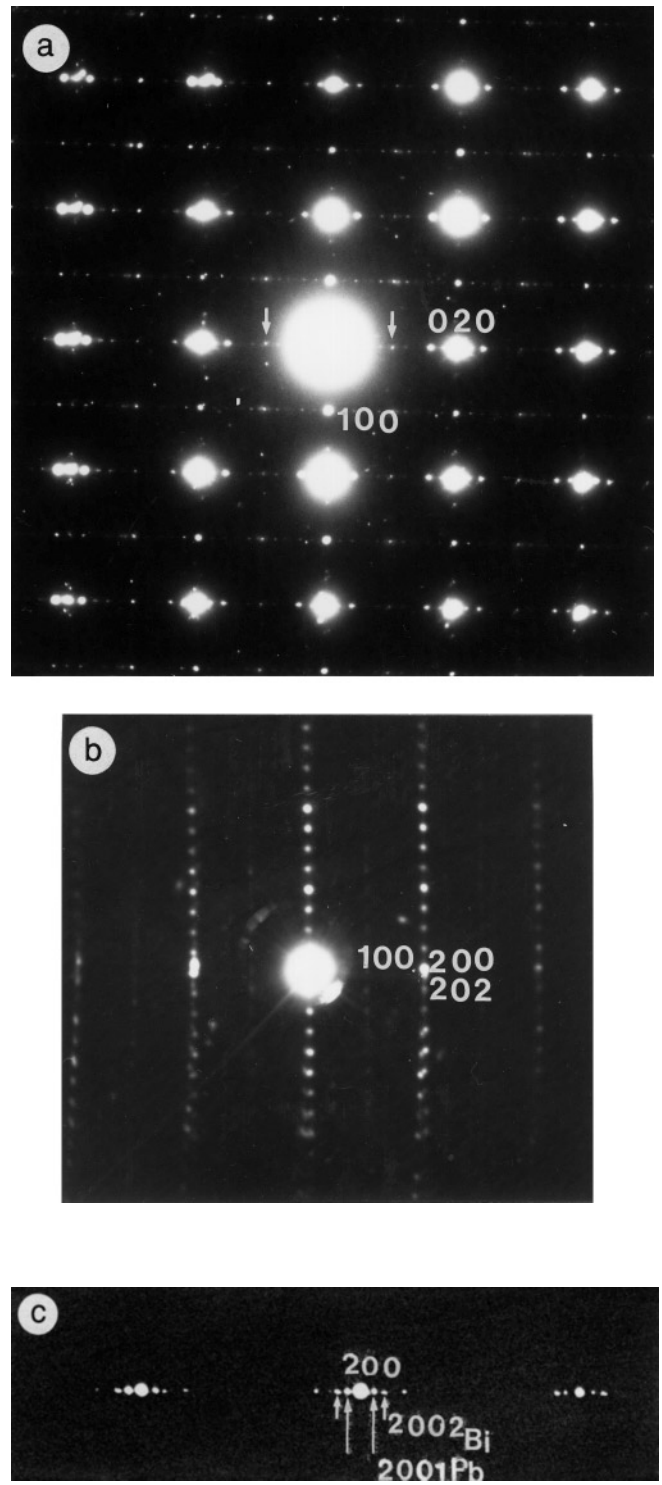

FIG. 1. $Bi_{1.5}Pb_{0.5}Sr_{1.5}Ca_{1.5}Mn_2O_{9-\delta}$: (a) [001] and (b) [010] ED patterns. The intense reflections are indexed in the A-type cell with $a \approx b \approx a_p\sqrt{2} \approx 5.4$ Å and $c \approx 31$ Å. The small white arrows indicate weak reflections with $0k0$, $k = 2n + 1$ which violate the A-type space group. (c) Enlargement of the [001] pattern showing the existence of two sets of satellites lying in incommensurate positions. Small white arrows show the satellites of the Bi-type modulation and the longer white arrows show the satellites of the Pb-type modulation.

TABLE 1

Refined Parameters of the Average Structure of $Bi_{1.5}Pb_{0.5}Sr_{1.5}Ca_{1.5}Mn_2O_{9-\delta}$, $a = 5.3594(1)$ Å, $b = 5.3443(1)$ Å, and $c = 30.976(4)$ Å, Space Group *Abmm* ($Z = 4$)

Atom and occupancy	Site	x	y	z
$Bi_{1.5}Pb_{0.5}$	8*m*	0.761(1)	0.0	0.0493(1)
$Sr_{0.7}Ca_{1.3}$	8*m*	0.75	0.5	0.1296(4)
$Sr_{0.83}Ca_{0.17}$	4*e*	0.75	0.5	0.25
Mn	8*m*	0.761(5)	0.0	0.1873(4)
O(1)	8*m*	0.871(8)	0.5	0.0493(1)
O(2)	8*m*	0.75	0.0	0.119(1)
O(3)	8*k*	0.5	0.25	0.1803(8)
O(4)	8*j*	0.0	0.25	0.1803(8)
O(5)	4*g*	0.75	0.0	0.25
Average positions calculated from reference 28 for $Bi_2Sr_3Fe_2O_9$				
Bi_2		0.767	0.009	0.047
Sr_2		0.746	0.506	0.131
Sr		0.749	0.5	0.257
Fe		0.746	0.002	0.194
O(1)		0.831	0.525	0.049
O(2)		0.75	0.009	0.115
O(3)		0.502	0.253	0.182
O(4)		0.010	0.252	0.183
O(5)		0.788	0.001	0.259

Two types of additional weak reflections are observed in the [001] pattern (Fig. 1a):

— the first are indicated by small white arrows. These extra spots correspond to the forbidden reflections with $k = 2n + 1$; their intensities are variable since they are scarcely visible for some of the grains. They violate the extinction conditions of an *A*-type lattice, involving a *P*-type space group. Such nonzero reflections have been reported for the bismuth cuprates and correlated to small local atoms displacements.

— the second group of extra reflections is that of a modulated structure. In fact, as reported by several authors for the Pb doped Bi oxides and oxycarbonates (16–20), there exist two types of modulations, which are both related to the existence of Bi contraction and Bi extension regions at the level of the [(Bi, Pb)O] layers. The Bi-type modulation produces out of phase waves whereas the Pb-type modulation produces in-phase waves of the [(Bi, Pb)O] planes (21–23). The incommensurate character of the Bi-type modulation is seen in Fig. 1a: the component of the wave vector along b^* is $q_{Bi} \approx 0.21b^* \approx b^*/4.8$. The intensity of the superstructure reflections strongly decreases with increasing order of the reflection; the second-order satellites are very weak. This value of the periodicity of the modulation is close to that usually observed in the undoped 2212 cuprate $Bi_2Sr_2CaCu_2O_{8\pm\delta}$ for which it was observed that the periodicity of the modulation varies with the oxygen content (24); the wave vector of the optimized superconducting cuprate $Bi_2Sr_2CaCu_2O_{8\pm\delta}$ ($T_c = 94$ K) is $0.207b^*$ (25–28). It is also similar to that observed in the iron-based 2212 phase which was observed ranging from 0.2 to 0.212 (1, 5, 6, 29). In Fig. 1c is an enlarged zone of the [001] pattern, surrounding the 200 reflection of the basic cell, recorded for a crystal where the two types of modulation are observed (short and long white arrows). The wave vector of the Bi type is $q_{Bi} \approx 0.21b^*$ and that the Pb type is $q_{Pb} \approx 0.12^*$. One satellite of each of the two systems is indexed using the *hklm* indices.

The electron diffraction investigation of the $Bi_{1.5}Pb_{0.5}Sr_{1.5}Ca_{1.5}Mn_2O_{9-\delta}$ oxide demonstrates that the basic cell and the modulated structure are similar to those observed in other Fe- and Cu- or Co-based 2212 systems. This emphasises the role of the distorted rock salt-type layers in the modulation phenomena.

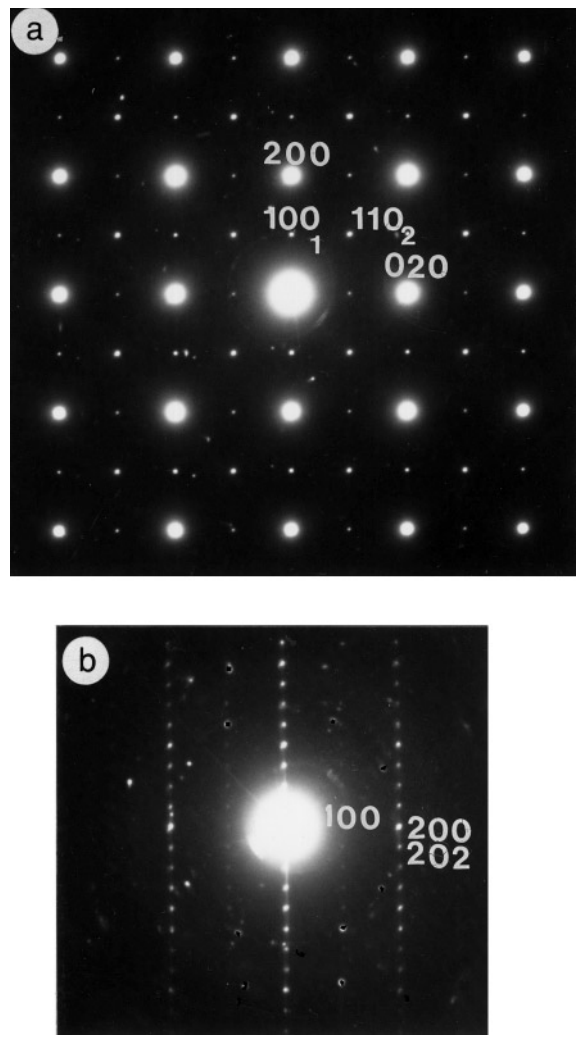

FIG. 2. $BiPbSr_{1.5}Ca_{1.5}Mn_2O_{9-\delta}$: (a) [001] ED pattern. The 100 and 110 reflections of each of the two variants are labeled 1 and 2, respectively. (b) [010] ED pattern.

$BiPbSr_{1.5}Ca_{1.5}Mn_2O_{9-\delta}$. For the majority of the crystallites of the Pb-rich oxide, one also observes systematically the superimposition of two systems but the structure is no longer modulated. This is illustrated in Fig. 2a for a typical [001] ED pattern. The first variant (labeled 1) corresponds to an orthorhombic basic cell similar to that observed for the above sample, i.e., *Abm*2 or *Abmm* (very weak 0*k*0 reflections with $k = 2n + 1$ are also observed); the [010] ED pattern is given in Fig. 2b. The second variant (labeled 2) is centered. The cell parameters were refined from the PXRD data to $a = 5.408(1)$ Å, $b = 5.322(1)$ Å, and $c = 30.979(5)$ Å.

Here again, the structural behavior is similar to that observed for the Pb-doped cuprates and oxycarbonates (16–20), where the modulated structure is no longer observed for the higher lead content.

High-Resolution Electron Microscopy and X-Ray Diffraction: The Average Structure

The [110] images of the layered bismuth materials correspond to the best orientation to understand the way the different layers are stacked along **c**. Similar [110] HREM images were observed for the two manganites. One example is given for $Bi_{1.5}Pb_{0.5}Sr_{1.5}Ca_{1.5}Mn_2O_{9-\delta}$ in Fig. 3a where the zone of high electron densities are highlighted. One observes two rows of staggered bright dots which are correlated to the two [(Bi, Pb)O] layers. These double layers are spaced 15.5 Å along **c** and shifted by $a_p/2$ along $[1\bar{1}0]$, in agreement with the *A*-type symmetry. Between two groups of double layers, one observes five rows of staggered grey dots, correlated to the [(Sr, Ca)O] layers and $[MnO_2]$ layers. The Bi and Mn layers are indicated by white and

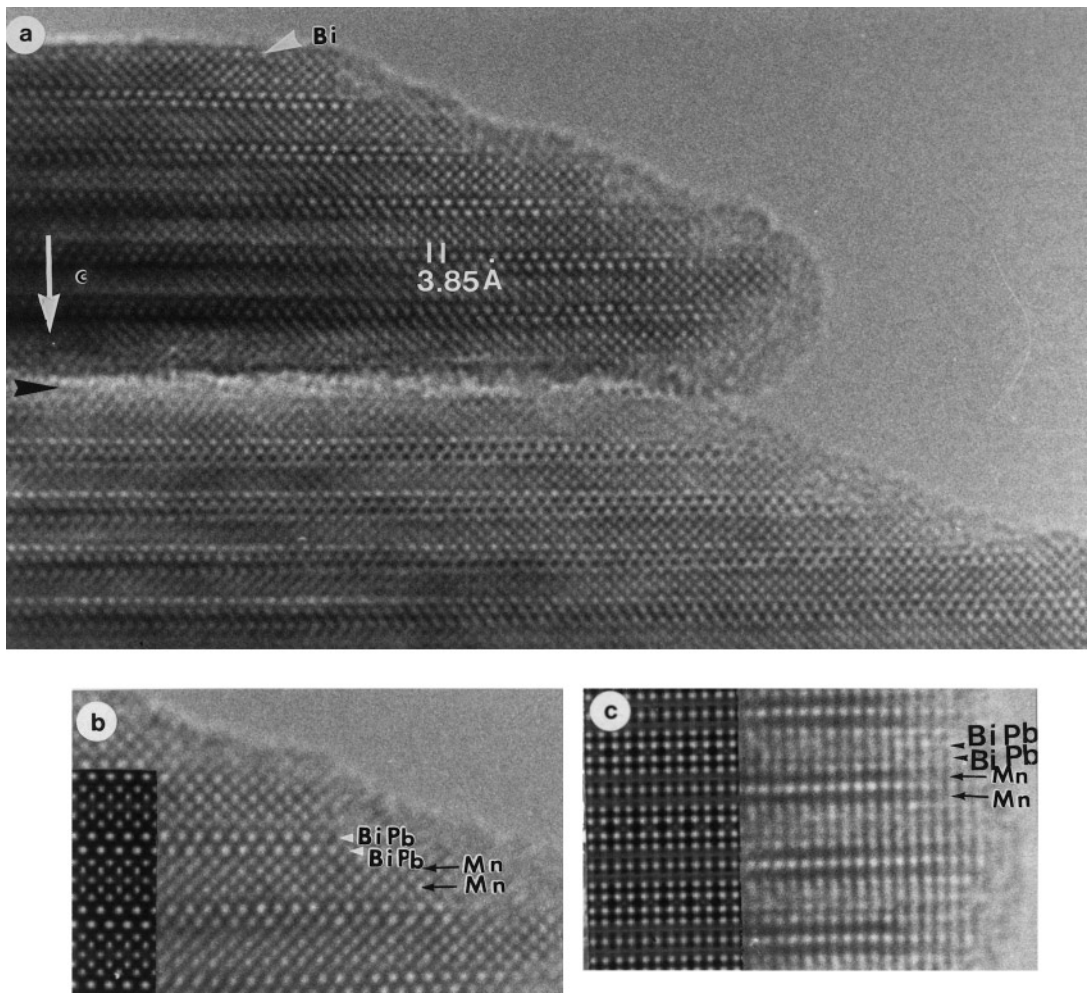

FIG. 3. HREM images of $Bi_{1.5}Pb_{0.5}Sr_{1.5}Ca_{1.5}Mn_2O_{9-\delta}$ illustrating the 2212-type average cell. (a) [110] overall image for which the cation positions appear as white dots. The black triangle shows the nature of one lamella boundary and the white triangle indicates that the cleavage arises between the two $[Bi_{1.5}Pb_{0.5}O]$ layers. (b) enlargement of the [110] image where the nature of the atoms is indicated. The calculated image is superimposed in the left part of the image. (Positional parameters are given in Table 1.) (c) [010] enlarged HREM image and corresponding calculated image.

black arrows, respectively, in the enlarged image in Fig. 3b. The following layer sequence can therefore be proposed:

$$[(Sr, Ca)O]\,[(Bi, Pb)O]\,[(Bi, Pb)O]\,[(Sr, Ca)O]\,[MnO_2]$$
$$[(Sr, Ca)O_{1-\delta}]\,[MnO_2]\,[(Sr, Ca)O].$$

This is in agreement with a 2212-type structure. The layer spacing measurement shows that the distances between the two $[MnO_2]$ layers within a perovskite slice is close to 3.9 Å, suggesting that the layer is not oxygen deficient like the 2212 cuprates but partially oxygenated, as in the Fe-based 2212 oxide (1–3, 6). The same spacing is indeed observed along [010], as shown in Fig. 3c where the cation positions appear as bright dots. The contrast of this image consists in a group of four bright dots ([(Sr, Ca)O] [(Bi Pb)O] [(Bi, Pb)O] [(Sr, Ca)O]) and a single dot separated by two rows of small grey dots, the $[MnO_2]$ layers. Note that the contrast of the single row, correlated to the $[(Sr, Ca)O_{1-\delta}]$ layer located between two $[MnO_2]$ layers, is as bright as the one of the rock salt layer, suggesting that the atomic positions are occupied by heavy cations, so that it contains mainly strontium.

On the basis of these observations, X-ray calculations were carried out for the average basic cell. The selected space group was *Abmm* and the starting atom positions were those usually considered for the Cu- and Fe-based Bi 2212's (6, 28, 30). The positional parameters, occupancy factors, and thermal factors of the cations were refined first; the positional parameters of the oxygen were refined in the second step, fixing their B factors to 1 Å^2.

Due to the close scattering factors of Bi and Pb, the Pb/Bi ratio was not refined. The Sr/Ca ratio was refined for the two types of sites, namely in the layers surrounding the double Bi layers and between the two manganese layers; they lead to an electron density which is in agreement with the EDS analyses and the HREM observations. A Sr/Ca ratio close to 4.9 is observed in the sites of the perovskite layer, i.e., between the MnO_2 layers and close to 0.5 in the other sites. This alkaline earth distribution is different from that observed in the cuprates were the calcium layer is located between the two copper layers. In the limits of accuracy of the refinement of such complex structure from powder XRD patterns, the oxygen occupancy of this layer ($\tau = 0.5 \pm 0.1$) suggests that it is partially oxygenated. The high Sr content and the presence of O within this layer are in agreement with the c parameter which is intermediate between $Bi_2Sr_2CaCu_2O_8$ and $Bi_2Sr_3Fe_2O_9$, that is, 30.52 and 31.69 Å, respectively. Although the R factor cannot be lowered below 0.12, due to the modulated and lamellar character of the structure, the average structural model (Fig. 4) is confirmed: the structure consists of double mixed layers involving both MnO_6 octahedra and MnO_5 pyramids, whose perovskite cages are

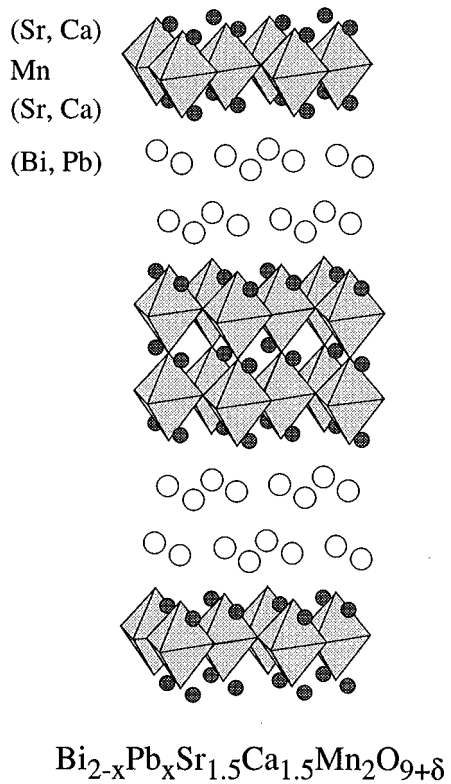

FIG. 4. Idealised structure of the 2212-type phase $Bi_{2-x}Pb_xSr_{1.5}Ca_{1.5}Mn_2O_{9-\delta}$.

mainly occupied by strontium (83% Sr, 17% Ca), intergrown with distorted triple rock salt layers, according to the cationic distribution $[Bi_{0.5}Pb_{0.5}\ Sr_{0.67}Ca_{1.33}]_{RS}$ $[Sr_{0.83}Ca_{0.17}]_PMn_2O_{8.5+\delta}$.

The refined positional parameters are given in Table 1. Note that these values are very close to those refined for the average structure of the $Bi_2Sr_3Fe_2O_9$ compound (Table 1). Image calculations were carried out from these values, varying the focus values and the crystal thicknesses. The simulated images fit well with the experimental ones. The images calculated for a focus value close to -600 Å and a crystal thickness of 15 Å are superimposed to the experimental images in Figs. 3b and 3c.

A [001] HREM image displayed in Fig. 5a illustrates the nonmodulated structure of $BiPbSr_{1.5}Ca_{1.5}Mn_2O_{9-\delta}$. The insertion of blocks of $4(\sqrt{2}/2)\ a_p$ and $5(\sqrt{2}/2)\ a_p$, arranged in a nonperiodic way in the 2201- and 2212-type modulated structures, is indeed no longer visible and one observes, for this compound, a very regular array of bright dots, spaced 2.7 Å, apart, along [100] and [010]. The contrast of the [010] image (Fig. 5b), recorded for this material, shows also clearly the 5.4 Å periodicity, similar to that observed in the Bi cuprates when the crystals are viewed along [010]. Such a contrast was correlated to the formation of Bi pairs due to the shift of the atoms parallel to the

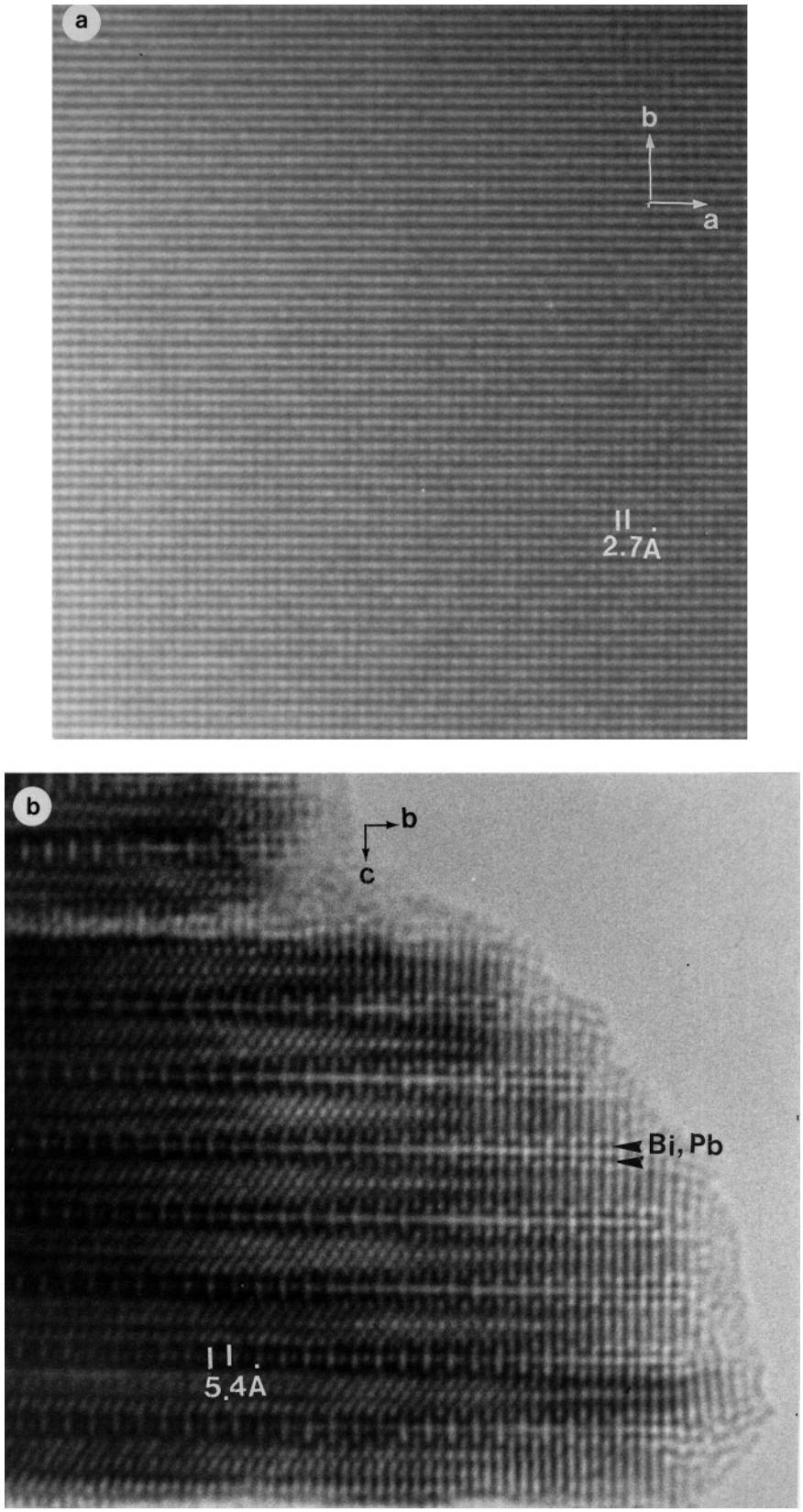

FIG. 5. HREM images of the oxide $BiPbSr_{1.5}Ca_{1.5}Mn_2O_{9-\delta}$: (a) [001] image showing the absence of modulation along [010]. (b) [010] image where the 5.4 Å periodicity clearly appears.

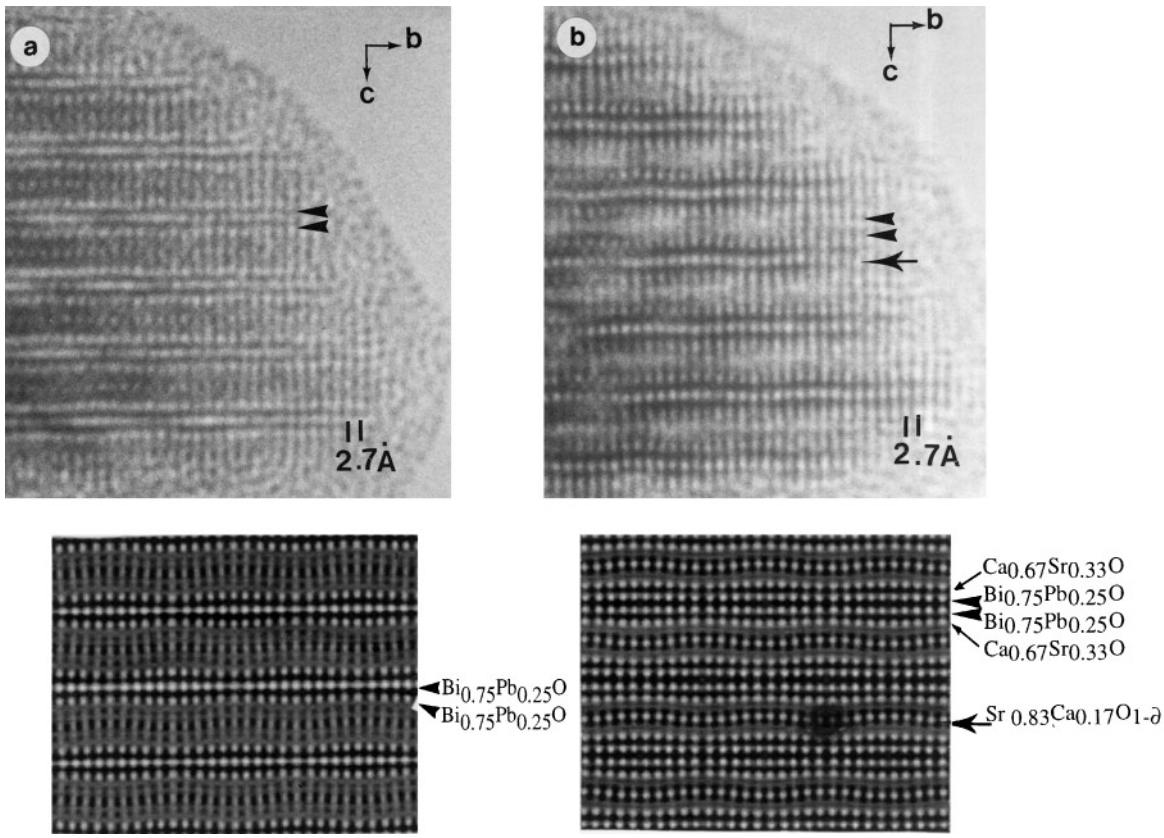

FIG. 6. Modulated structure of $Bi_{1.5}Pb_{0.5}Sr_{1.5}Ca_{1.5}Mn_2O_{9-\delta}$: [100] images recorded for focus values assumed to be closed to (a) -300 Å where the cation positions appear as dark dots and (b) -600 Å where they are imaged as bright dots. Simulated images were calculated with the help of positional parameters adapted from the Fe-based compound (28). (c) Overall image where the two rows of brighter dots are correlated to the $[Ca_{0.67}Sr_{0.33}O]$ layers. The small white triangles indicate zones where the modulation vector varies. (d) Projection along [100] of the atom positions of the modulated structure used for the image calculations in Figs. 6a, 6b and 6c.

[100] direction with regard to the special positions [31]. This effect is very intense in the $BiPbSr_{1.5}Ca_{1.5}Mn_2O_{9-\delta}$ compound. Some deviations from the perfect agreement, in the form of a shifting of $a/2$, is observed in the manganites as in the Bi cuprates (31) and oxycarbonates (20).

Modulated Structure of $Bi_{1.5}Pb_{0.5}Sr_{1.5}Ca_{1.5}Mn_2O_{9-\delta}$

As described in the electron diffraction section, $Bi_{1.5}Pb_{0.5}Sr_{1.5}Ca_{1.5}Mn_2O_{9-\delta}$ exhibits an incommensurate structure. The [100] HREM images allow us to visualize these modulations. Three images are given in Figs. 6a, 6b, and 6c, recorded for different focus values. The first enlarged image (Fig. 6a) corresponds to a focus close to the Scherzer value, -300 Å, where the zones of light electron density are highlighted; the second enlarged image of the same area (Fig. 6b) corresponds to a focus close to -600 Å, where the cations positions appear as bright dots. Last, in the overall image of Fig. 6c, only the two $[Sr_{0.33}Ca_{0.67}O]$ layers appear as two rows of bright dots (focus value close to -150 Å).

The first two images (Figs. 6a and 6b) show clearly that, in this area, two successive $[Bi_{1.5}Pb_{0.5}O_2]$ layers undulate in phase opposition and that the image is centered. This corresponds to a Bi-type modulation. In Fig. 6b, the undulation of the $[Sr_{0.83}Ca_{0.17}O_{0.5}]$ layer is easily observed, as well as that of the two $[Sr_{0.33}Ca_{0.67}O]$ layers in Fig. 6c. Taking into account that the modulation vector of the $Bi_2Sr_3Fe_2O_9$ compound is the same as that of $Bi_{1.5}Pb_{0.5}Sr_{1.5}Ca_{1.5}Mn_2O_{9-\delta}$, image simulations were carried out, adapting the positional parameters and site compositions of the Fe-based oxide (28) to the Mn-based one (Fig. 6d). They are compared to each of the experimental images in Fig. 6, enhancing the similarity between the two 2212 members.

Two remarks can be made about this modulated structure. First, as previously reported in the Bi cuprates, the out of phase waving of the Bi layers is not always perfect an a variation of modulation vectors may locally occur (see as an example the small white arrows in Fig. 6c). As a result, the *A*-centered orthorhombic symmetry of the modulated structure is locally destroyed as previously mentioned for the Bi oxycarbonates (20, 32), and the structure is locally

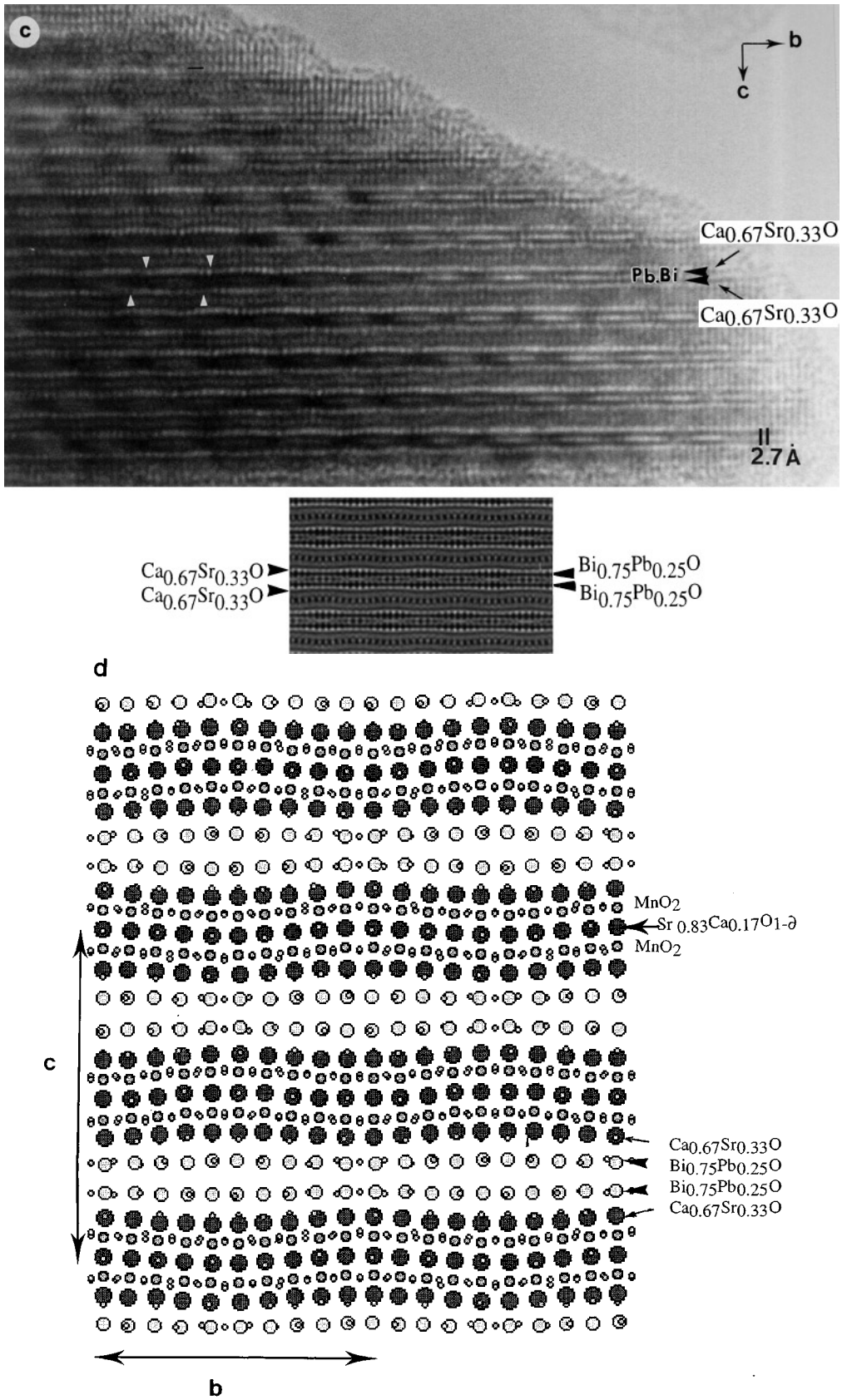

FIG. 6—*Continued*

monoclinic. Such an effect has been observed in the pure Bi cuprates but in the present sample it could be favored by the existence of mixed Bi/Pb layers which do not exhibit the same type of modulation. Consequently it may arise from weak Pb/Bi inhomogeneous distributions within the rock salt layers.

The second point deals with the coincidence of the wavelength and the composition of the strongly undulating [$Sr_{0.83}Ca_{0.17}O_{0.5}$] layer. Single crystal X-ray diffraction data would be essential to refine the modulated structure and test an eventual preferential position of the calcium with regard to the Sr in this layer.

Morphology and Cleavage

The ED and HREM study showed that the Mn-based 2212 components exhibit a mica-like morphology, which is similar to that observed in the other Bi layered compounds. The crystals consist of lamella which are a few tens of nanometers thick stacked along [001]. The cleavage of the crystal occurs, as usually, between the two Bi layers (Fig. 3a). The formation of the lamella is often originated by a strong atomic disordering at the level of the Bi layers (see for an example Fig. 3a where the junction is indicated by a black arrowhead).

As in the Cu- and Fe-based Bi 2212's, the superimposition of 90° oriented domains ([100] and [010]) and slight disorientation of adjacent lamella by rotation with respect to the other around [001] are often observed, but contrary to the latter's, the existence of 45° oriented domains are also observed in the 2212 manganites. An example is given in Fig. 7. The electron diffraction pattern (Fig. 7b) and the HREM image (Fig. 7a) show that the [100] and [110] lamella are stacked with a common c axis. The junction between the two lamella is not strongly disturbed suggesting a structural origin to the phenomenon such as the oxygen distribution at the level of a single layer, since 45° is the angle between the perovskite and the rock salt networks.

Defective Structure

In $Bi_{1.5}Pb_{0.5}Sr_{1.5}Ca_{1.5}Mn_2O_{9-\delta}$, few intergrowth defects are observed. A rare example is displayed in Fig. 8. This

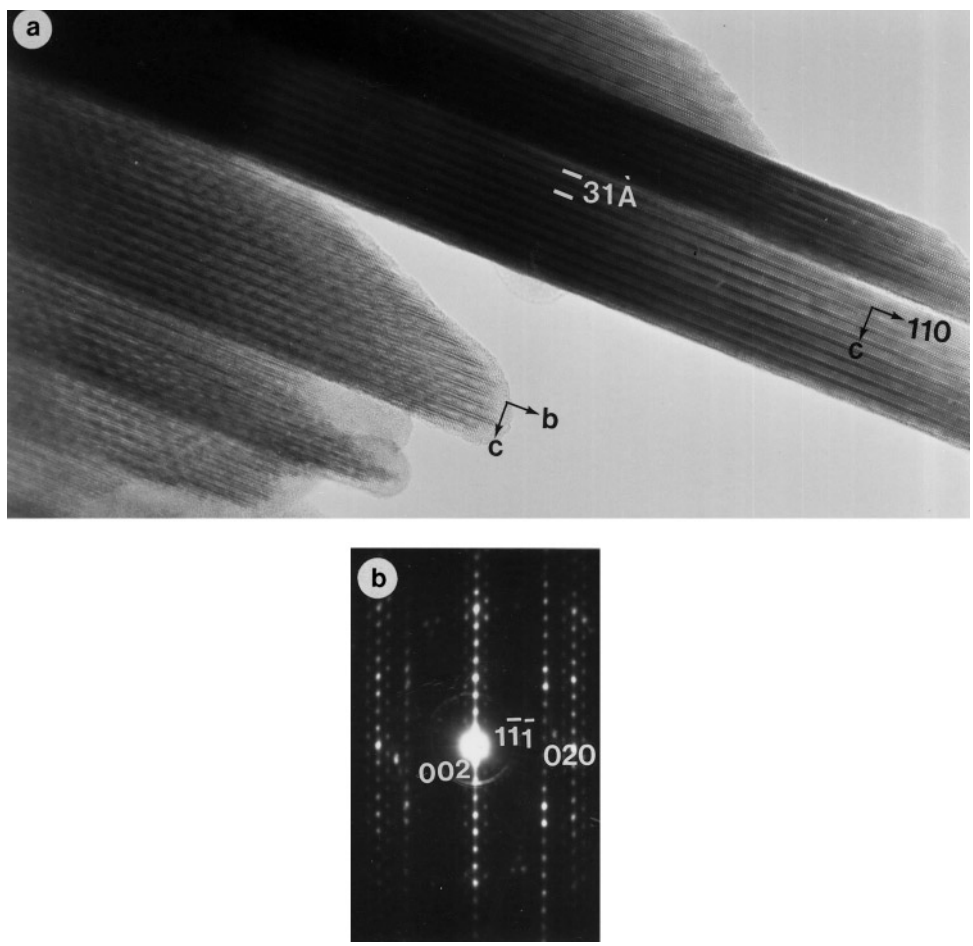

FIG. 7. $Bi_{1.5}Pb_{0.5}Sr_{1.5}Ca_{1.5}Mn_2O_{9-\delta}$: (a) image and (b) corresponding ED pattern of a grain where 45° oriented lamella are observed.

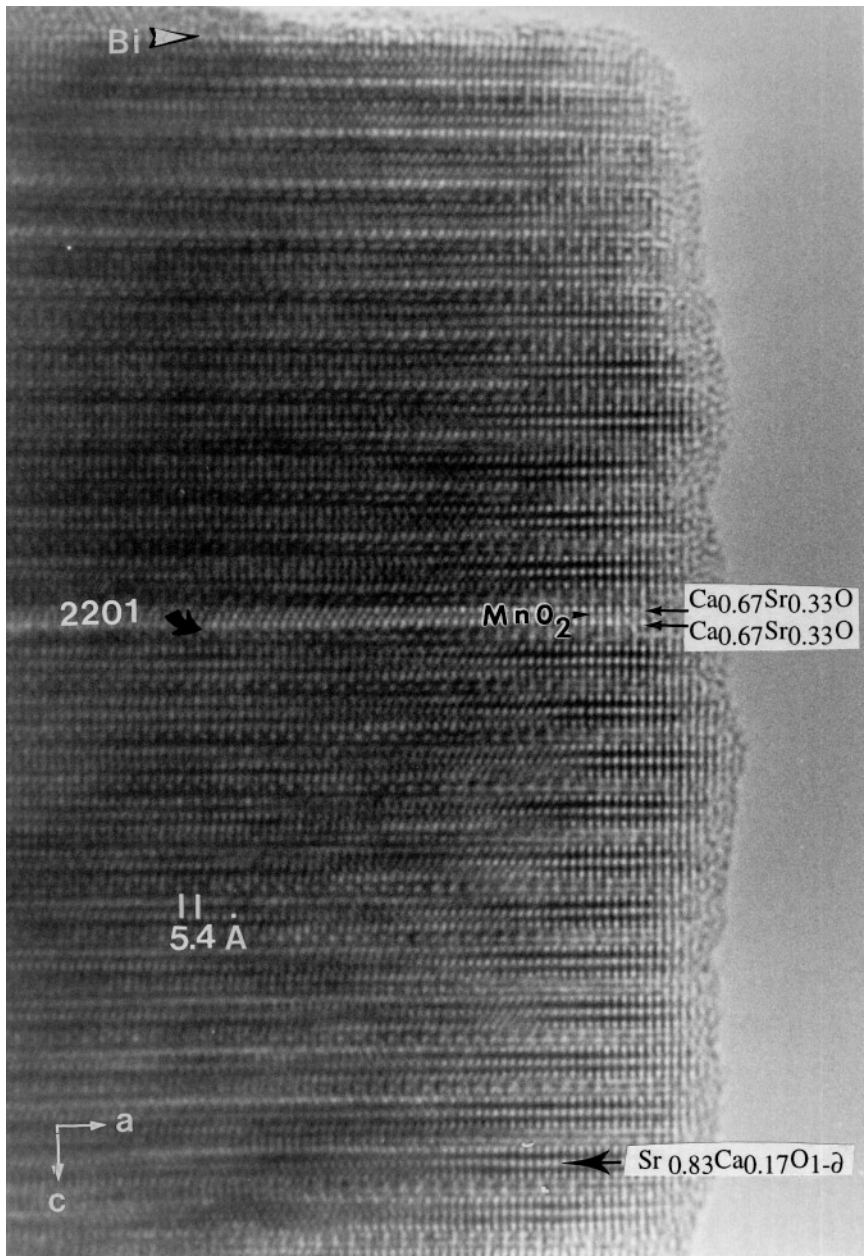

FIG. 8. Example of 2201 defective number (curved arrow) in a regular crystal of $Bi_{1.5}Pb_{0.5}Sr_{1.5}Ca_{1.5}Mn_2O_{9-\delta}$. The white triangle outlines the cleavage occurs at the level of the bismuth layer.

[010] image was recorded for a focus value where the cation positions appear as bright dots. At the level of the defective member, one clearly observes two adjacent rows of bright dots, spaced 3.9 Å apart. This is associated with the formation of a 2201 member, $Bi_{2-x}Pb_xSr_2MnO_6$ (15).

In $BiPbSr_{1.5}Ca_{1.5}Mn_2O_{9-\delta}$, the existence of stacking defects is more frequent. Diffuse streaks are observed along the c^* direction as shown in the [110] electron diffraction pattern displayed in Fig. 9a. The corresponding overall image (Fig. 9b) shows that there exist stacking defects and distortions of the matrix. In the enlarged image of a part of the crystal edge (Fig. 9c), it is clear that several non-stoichiometry mechanisms occur. First, 2201, 2212, and 2223 members are stacked in the disordered way (they are indicated by the m values, respectively, 1, 2, and 3 [MnO_2] layers). A second type of defect corresponds to the stopping of the rock salt layers (large black arrowhead) within the matrix. The three rock salt layers are replaced by two perovskite slices so that two 2212 members are transformed in a local $m = 6$ member. The idealized drawing of the defect is given in Fig. 9d. In some places, the substitution is not complete and one rock salt layer out of three is retained. An

example is indicated by a black arrow and the two [AO] layers forming the single rock salt layer are shown by the two small black triangles. As a consequecne, a local 0223 member is formed. The idealized drawing of such a defect is given in Fig. 9e.

Such complex features are indeed a consequence of an inhomogeneous distribution of the cations within the matrix and the fact that the Bi and the Ca are able to occupy the octahedral site of a perovskite framework.

Electrical Properties

The variation of the resistance as a function of $1/T$ is given in Fig. 10 for the two $Bi_{1.5}Pb_{0.5}Sr_{1.5}Ca_{1.5}Mn_2O_{9-\delta}$ and $BiPbSr_{1.5}Ca_{1.5}Mn_2O_{9-\delta}$ manganites. The room temperature resistivity is large and the resistance decreases with increasing temperature, indicating semiconducting behavior. The data are fitted to an Arrhenius law, leading to an activation energy of 0.15 eV for $Bi_{1.5}Pb_{0.5}Sr_{1.5}Ca_{1.5}Mn_2O_{9-\delta}$ and 0.18 eV for $BiPbSr_{1.5}Ca_{1.5}Mn_2O_{9-\delta}$. The resistivity of the lead-rich compound ($x = 1$) is one order of magnitude higher than that of the Bi-rich compound ($x = 0.5$).

CONCLUDING REMARKS

This study shows that a manganite with the "2212" structure can be synthesized. Nevertheless it is worth pointing out that its stabilization requires a large calcium content compared to the "2212" bismuth cuprate $Bi_2Sr_2CaCu_2O_{8+\delta}$ or to the iron-based phase $Bi_2Sr_3Fe_2O_{9+\delta}$. The presence of lead in the structure also seems to be an important factor for the stabilization of the structure, since no trace of the "2212" phase could be detected for the pure bismuth compositions $Bi_2Sr_{3-x}Ca_xMn_2O_{9-\delta}$, whatever x.

The first important characteristic of this phase concerns the fact that the $x = 0.5$ compound exhibits a modulated structure similar to those of the copper and iron phases, with a q vector similar to that of $Bi_2Sr_3Fe_2O_{9-\delta}$ (6). The second important feature concerns the distribution of the calcium and strontium cations. One indeed observes a preferential occupancy of the distorted rock salt layers by

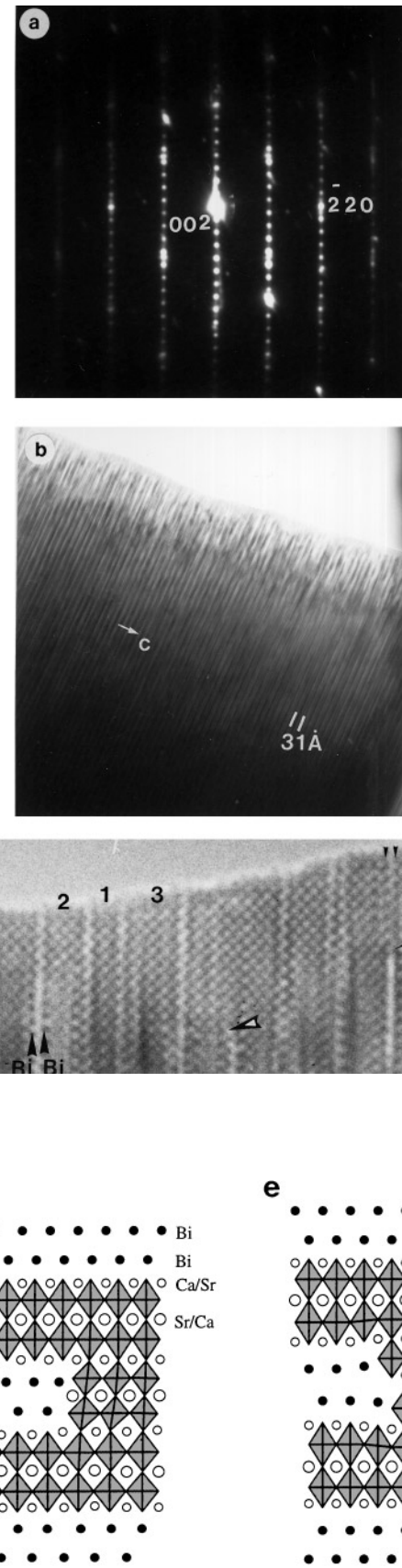

FIG. 9. $BiPbSr_{1.5}Ca_{1.5}Mn_2O_{9-\delta}$: (a) [110] ED pattern showing diffuse streaks along [001]* and (b) corresponding overall image. (c) Enlargement of the crystal edge illustrating the different nonstoichiometry features. The cation positions appear as dark dots (the two [(Bi, Pb)O] layers are shown by black triangles). The black numbering indicates the number of $[MnO_2]$ layers of the different numbers stacked along [001]: **1** for 2201 and **3** for 2223, that of the regular matrix being **2** (2212). The black and white triangle shows the stopping of the rock salt layers which are replaced by perovskite-type layers (model in Fig. 9d), leading locally to a $m =$ **6** member. The local information on one 0223 defective member is indicated by a black arrow and the corresponding model in Fig. 9e.

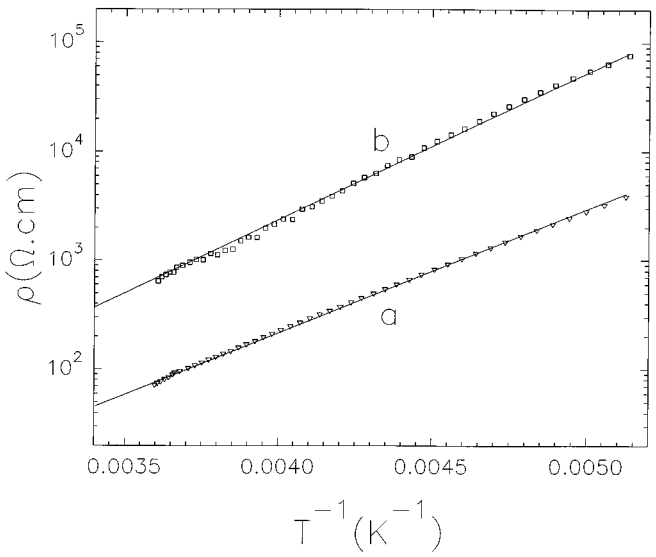

FIG. 10. Variation of the resistivity as a function of $1/T$: (a) corresponds to $Bi_{1.5}Pb_{0.5}Sr_{1.5}Ca_{1.5}Mn_2O_{9-\delta}$ and (b) to $BiPbSr_{1.5}Ca_{1.5}Mn_2O_{9-\delta}$.

calcium and of the perovskite cages of the double perovskite layers by strontium.

It is worth pointing out that the present study does not allow the exact oxygen content to be determined. Consequently, as for the study of $Bi_2Sr_2MnO_{6+\delta}$ (7), the exact valence of manganese cannot be discussed. Nevertheless it is most probable that most of the manganese exhibits the trivalent state, if one considers the ideal chemical formula. A neutron diffraction investigation will be necessary to shed light on this issue.

Taking into consideration the GMR properties of the manganese perovskites, it will be of high interest to study the magnetic properties of these compounds. Unfortunately the presence of impurities prevents a serious study. Soft chemistry techniques (see for a review (33)) should offer an interesting alternative and are in progress to prepare a pure phase.

REFERENCES

1. M. Hervieu, C. Michel, N. Nguyen, R. Retoux, and B. Raveau, *Eur. J. Solid State Inorg. Chem.* **25,** 375 (1988).
2. R. Retoux, C. Michel, M. Hervieu, N. Nguyen, and B. Raveau, *Solid State Commun.* **69,** 599 (1989).
3. J. M. Tarascon, P. F. Micelli, P. Barboux, D. M. Hwang, G. W. Hull, M. Giroud, L. H. Greene, Y. Le Page, W. R. McKinnon, E. Tselapis, G. Pleigier, M. Eischutz, D. A. Neumann, and J. J. Rhyne, *Phys. Rev. B* **39,** 11587 (1989).
4. J. M. Tarascon, R. Ramesh, P. Barboux, M. S. Hedge, G. W. Hull, L. H. Greene, M. Giroud, Y. Lepage, and W. R. McKinnon, *Solid State Commun.* **71,** 663 (1989).
5. J. M. Tarascon, Y. Lepage, W. R. McKinnon, E. Tselepis, P. Barboux, B. G. Bagley, and R. Ramesh, *Mater. Res. Soc. Pittsburgh PA*, 317 (1989).
6. O. Pérez, H. Leligny, D. Grébille, J. M. Grenêche, Ph. Labbé, D. Groult, and B. Raveau, *Phys. Rev. B* **55**(2), 1236 (1997).
7. W. R. McKinnon, E. Tselepis, Y. Lepage, S. P. McAlister, G. Pleitzier, J. M. Tarascon, P. F. Miceli, R. Ramesh, G. W. Hull, J. V. Waszczak, J. J. Rhyne, and D. A. Neumann, *Phys. Rev. B* **41,** 4489 (1990).
8. R. M. Kusters, J. Singleton, D. A. Keon, R. M. Greedy, and W. Huges, *Physica B* **155,** 362 (1989).
9. R. Von Helmolt, J. Wecker, B. Holzapfel, L. Schultz, and K. Samwer, *Phys. Rev. Lett.* **71,** 2331 (1993).
10. H. L. Ju, C. Kwon, Q. Li, R. L. Greene, and T. Venkatessen, *Appl. Phys. Lett.* **65,** 2108 (1994).
11. A. Maignan, V. Caignaert, C. Simon, M. Hervieu, and B. Raveau, *J. Mater. Chem.* **5,** 1089 (1995); A. Maignan, C. Simon, V. Caignaert, and B. Raveau, *Solid State Commun.* **96,** 623 (1995).
12. Y. Morimoto, A. Asamitsu, H. Kuwahara, and Y. Tokura, *Nature* (*London*) **380,** 141 (1996); P. Laffez, G. Van Tendeloo, R. Seshadri, M. Hervieu, C. Martin, A. Maignan, and B. Reveau, *J. Appl. Phys.* **80,** 5850 (1996); R. Seshadri, C. Martin, A. Maignan, M. Hervieu, B. Raveau, and C. N. R. Rao, *J. Mater. Chem.* **6,** 1585 (1996).
13. H. M. Rietveld, *Acta Crystallogr.* **22,** 151 (1967).
14. J. Rodriguez-Carjaval, *in* "Collected Abstracts of Powder Diffraction Meeting, Toulouse, France, July 1990" (J Galy, Ed.,) p. 127.
15. J. M. Tarascon, Y. Lepage, W. R. McKinnon, R. Ramesh, M. Eibschutz, E. Tselepis, E. Wang, and G. W. Hull, *Physica C* **167,** 20 (1990).
16. J. M. Tarascon, W. R. McKinnon, Y. Lepage, K. Remshing, R. Ramesh, R. Jones, G. Pleizre, and G. W. Hull, *Physica C* **172,** 13 (1990).
17. J. Schneck, J. C. Toledano, L. Pierre, A. Litzer, D. Morin, J. Prinmot, H. Savary, and C. Daguet, *J. Less Common Metals* **545,** 164–165 (1990).
18. O. Eibl, *Physica C* **175,** 419 (1991).
19. D. Pelloquin, M. T. Caldes, C. Michel, A. Maignan, M. Hervieu, and B. Raveau, *Physica C* **214,** 87 (1993).
20. X. F. Zhang, G. Van Tendeloo, S. Amelinckx, D. Pelloquin, C. Michel, M. Hervieu, and B. Raveau, *J. Solid State Chem.* **113,** 327 (1994).
21. H. W. Zandbergen, W. A. Groen, A. Smit, and G. Van Tendeloo, *Physica C* **168,** 426 (1990).
22. Y. Matsui and S. Horiuchi, *Jpn. J. Appl. Phys.* **28,** L946 (1989).
23. O. Eibl, *Physica C* **168,** 215 (1990).
24. A. Q. Pham, M. Hervieu, A. Maignan, C. Michel, J. Provost, and B. Raveau, *Physica C* **194,** 243 (1992).
25. H. W. Zandbergen and P. Groen, *Solid State Comm.* **66,** 97 (1988).
26. M. Hervieu, C. Michel, B. Domengès, Y. Laligant, A. Lebail, G. Ferey, and B. Raveau, *Mod. Phys. Lett. B* **2,** 491 (1988).
27. H. W. Zandbergen, W. A. Groen, F. C. Mijhoff, G. Van Tendeloo, and S. Amelinckx, *Physica C* **156,** 325 (1988).
28. Y. Lepage, W. R. McKinnon, J. M. Tarascon, and P. Barboux, *Phys. Rev. B* **40,** 6810 (1989).
29. J. M. Tarascon, Y. Lepage, and W. R. McKinnon, *Eur. J. Solid State Inorg. Chem.* **27,** 82 (1990).
30. H. Maeda, Y. Tanaka, M. Fukutomi, and T. Asano, *Jpn. J. Appl. Phys.* **27**L, 209 (1988).
31. H Budin, O. Eibl, P. Pongratz, and P. Skalicky, *Physica C* **207,** 208 (1993).
32. M. Hervieu, M. T. Caldes, C. Michel, D. Pelloquin, and B. Raveau, *J. Solid State Chem.* **108,** 346 (1994).
33. J. Gopalakrishnan, *Chem. Mater.* **7**(7), 1265 (1995).